CONFIDENTIAL

HYDRODYNAMIC CHARACTERISTICS OF THE 12.75 INCH TYPE X10 ANTISUBMARINE ROCKET

REPORT NO. N-53

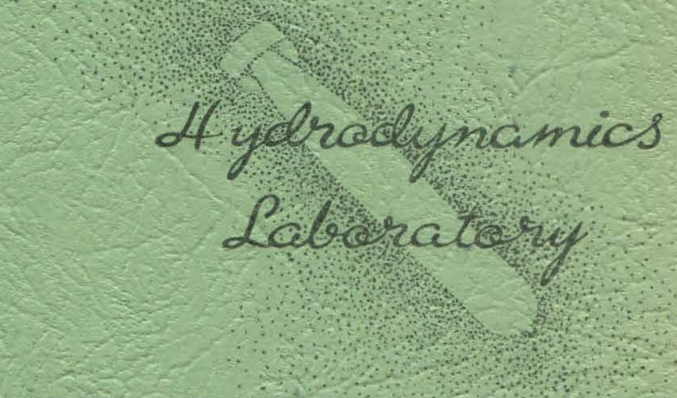

CALIFORNIA INSTITUTE OF TECHNOLOGY - PASADENA CALIFORNIA

U.S. NAVY BUREAU OF ORDNANCE CONTRACT NOrd 9612

CONFIDENTIAL

NAVY DEPARTMENT
BUREAU OF ORDNANCE
CONTRACT NORD 9612

HYDRODYNAMIC CHARACTERISTICS

OF THE

12.75-INCH TYPE X10 ANTISUBMARINE ROCKET

ROBERT T. KNAPP
DIRECTOR

HYDRODYNAMICS LABORATORY
CALIFORNIA INSTITUTE OF TECHNOLOGY
PASADENA, CALIFORNIA

Laboratory Report No. N-53
October 22, 1947

Report Prepared by
Gerald B. Robison
Hydraulic Engineer

COPY NO. 5

CONTENTS

SUMMARY AND CONCLUSIONS

Part I

Reported herein are tests of the 12.75-inch Type X 10 Anti-submarine Rocket to determine hydrodynamic force coefficients, both without cavitation and in a full cavitation bubble; incipient cavitation characteristics; and flow conditions as revealed in the Polarized Light Flume.

Conclusions

1. Variations in force coefficient values may amount to $\pm$ 3 per cent in carefully manufactured models and are an indication of greater variations to be expected from projectiles produced by normal methods.

2. For noncavitating conditions and a Reynolds number of 4×10^6, the drag coefficient was 0.261 at zero yaw; the cross force and moment (about center of gravity) coefficients, 0.57 and -0.12 at 10 degrees of yaw, respectively. The extrapolated drag coefficient for the prototype at $R = 23.6 \times 10^6$ gives a terminal velocity of 35.2 feet or 36.8 feet per second, depending upon absence or presence of water in the discharged motor tube.

3. Steady incipient cavitation occurred as follows:

Location	K Value
Nose	1.80
Inside leading edge tail ring	1.26
Outside ring, junction with fins	0.80
Complete outside leading edge of ring	0.64
Afterbody cavitation was obscured by bubble from nose	

4. With full cavitation bubble, the drag coefficient was 0.40 at zero yaw; the cross force coefficient, -0.06 at +4 degrees; and the moment coefficient appeared to be zero within the yaws of $\pm$ 4 degrees.

5. Flow line studies gave no unexpected results. There is a marked zone of disturbance immediately aft of the nose and a notably small afterbody disturbance due to its streamlined form.

Part II

This laboratory was requested to recommend a nose design for the 12.75-inch Antisubmarine Rocket which would give a terminal velocity of 40 feet per second. Such a nose was to have a flat face with a diameter not less than half the projectile diameter.

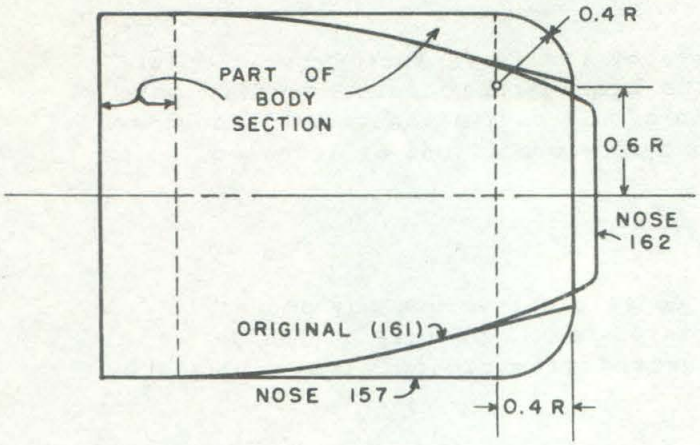

DIMENSIONS FOR NOSE 157, ONLY

COMPARATIVE OUTLINES OF ORIGINAL AND SUGGESTED DESIGN NOSES FOR 12.75-INCH AS ROCKET

Two designs are submitted herein. The diagram shows their outlines together with that of the original nose. Calculations indicate that either should give a terminal velocity between 47 and 48 feet per second in sea water of 60° Fahrenheit (with 23.7 lbs. of water in discharged motor tube, 45 ft/sec if empty). These nose shapes are sufficiently different to afford considerable latitude in respect to characteristics of maximum range, ricochet, cavitation, and performance in the entry bubble.

It is unlikely that any other nose shape could further materially reduce the drag while other components remain unchanged.

The new noses have trivial effect on the cross force coefficient developed with the original nose and all have considerable static stability.

HYDRODYNAMIC CHARACTERISTICS OF THE 12.75-INCH TYPE X1O ANTISUBMARINE ROCKET

GENERAL

This report is divided into two parts. Part I covers investigations made in conformity with a letter dated June 27, 1946, from Vice Admiral G. F. Hussey, Jr. to Dr. Knapp. Part II deals with additional investigations requested by Admiral Hussey in a letter dated September 17, 1946. All work was performed under Contract NOrd 9612 in the Hydrodynamics Laboratory of the California Institute of Technology.

PART I

PURPOSE

The purpose of the original investigation was to determine the hydrodynamic force coefficients of the 12.75-inch Type X1O Antisubmarine Rocket, both without cavitation and in a full cavitation bubble; the incipient cavitation characteristics; and to study the flow around the projectile in the Polarized Light Flume.

PHYSICAL DATA

Physical data relating to the prototype were given as follows:

Over-all length	97.587 inches = 8.132 feet
Distance from nose to C.G.	36.000 inches = 3.000 feet
Maximum diameter	12.750 inches = 1.0625 feet
Area at maximum cross section	127.68 sq. in. = 0.888 sq. ft.
Diameter of nose face	7.876 inches = 0.656 foot
Wt/in.^{2} of area at maximum cross section (in fresh water)	2.22 lbs.
Weight, loaded	525.2 lbs.
after firing	504.0 lbs.
propellant	20.92 lbs.
inert components	0.28 lb.
Estimated velocity (in air)	293 ft/sec
Maximum range	800 yds.
Spin in water	2.1 rps
Sinking rate	40 ft/sec

Model data:

Diameter	2.000 inches
Length, over-all	15.308 inches
Distance, nose to C.G.	5.647 inches
Nose to support point	5.247 inches
Scale ratio	1 to 6.375

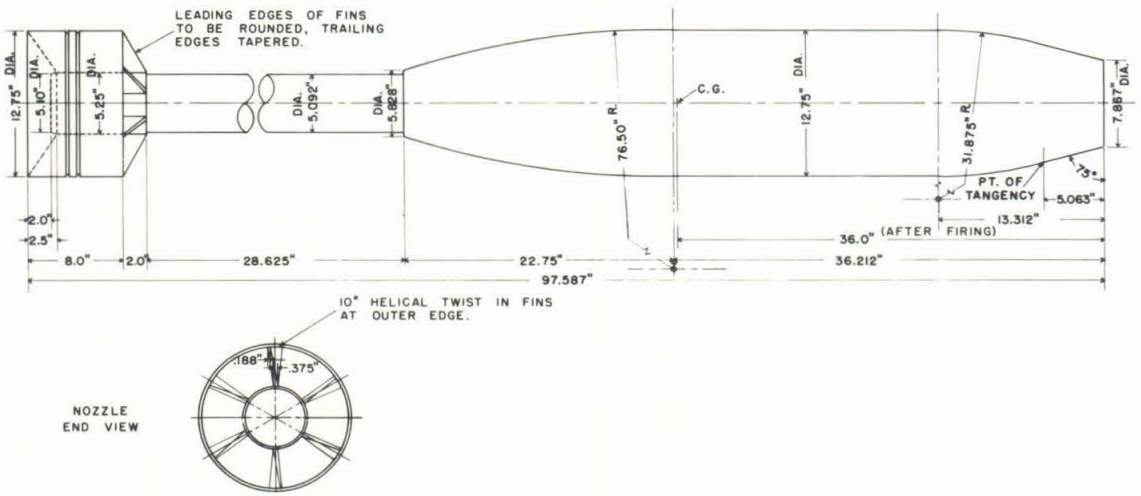

FIG. 1 – OUTLINE OF 12.75–INCH TYPE X10 ANTISUBMARINE ROCKET

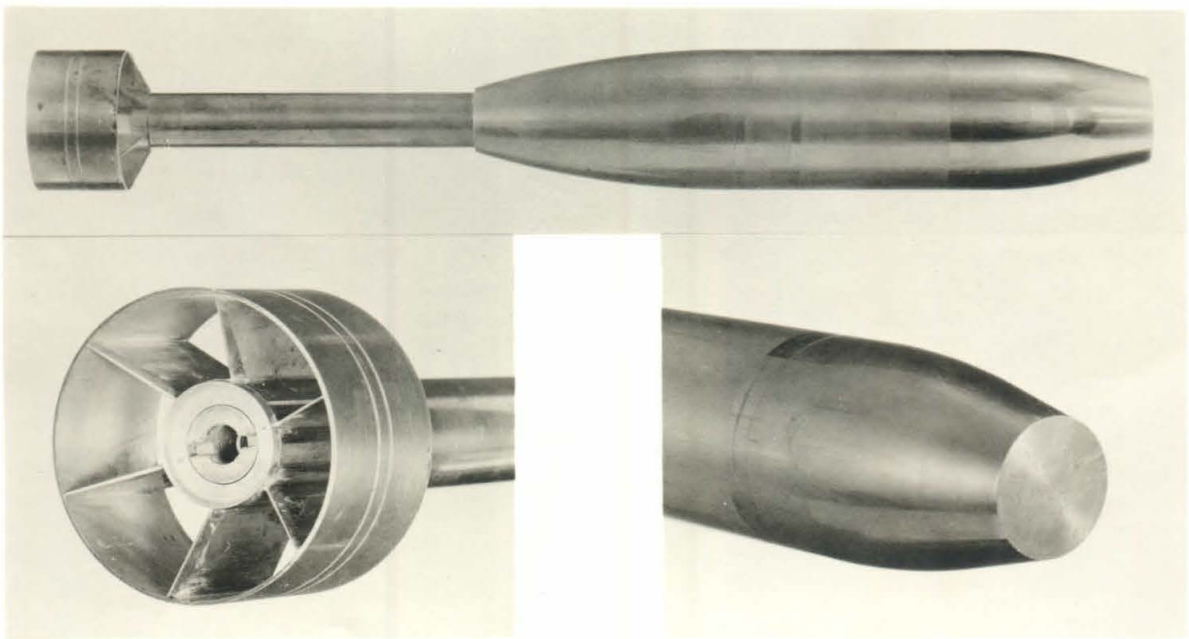

FIG. 2 – GENERAL VIEW OF 2–INCH DIAMETER MODEL OF THE 12.75–INCH TYPE X10 ANTISUBMARINE ROCKET WITH DETAIL VIEWS OF NOSE AND TAIL

Figure 1 is a general outline drawing of the prototype. Figure 2 is a general view of the model together with detail views of the nose and tail. The prototype tail vanes have a 10-degree helical twist at their outer edges. The model tail vanes were purely radial since the model must be in a fixed position for tests.

TEST CONDITIONS AND RESULTS

Noncavitation Force Coefficients

Force tests for noncavitating conditions were made with a velocity of 32 ft/sec corresponding to a Reynolds number of approximately four million. The support point was 34.3 per cent of the model length aft of the nose face. All data were corrected for support shield interference and the drag coefficient was reduced 0.015 by a horizontal buoyancy correction. Yaw runs were made to $\pm$ 10 degrees with the model at zero index and repeated at 45 degrees index. (The tail zero index had one pair of vanes vertical. The relationship of the tail to the remainder of the model was not changed when the model was at 45 degrees index.) The plus and minus readings for a given angle were averaged in order to eliminate the effect of any unintentional asymmetries in the model. Such variations may amount to $\pm$ 3 per cent in carefully manufactured models and are an indication of greater variations which could be expected with projectiles produced by normal methods.

Figure 3 shows the influence of yaw angles on the drag, cross force and moment (about the center of gravity) coefficients to 10 degrees. Drag coefficient values are, of course, positive for both plus and minus angles; cross force coefficient values have the same sign as the angle and, in this case, the moment coefficient values have the opposite sign.

The British Squid was more nearly like this projectile than any other tested here. Its outline is shown in Figure 4.* It has a similar blunt nose and an eight-vane ring tail with a boom hardly larger than the tail hub. Its length to diameter ratio, however, was only 4.625 as compared to 7.65 for the subject model. The drag coefficient for the Squid was well established at 0.175 compared to 0.261 for the 12.75-inch Antisubmarine Rocket, both at Reynolds number 4,000,000. The higher value for the rocket is only partly attributable to the increased skin friction drag. The skin friction drag coefficient, on the assumption that it is the same as that for a flat plate of the same length and surface area, was 0.079 for the Squid, leaving 0.096 for the form drag coefficient. The skin friction drag coefficient for this rocket is approximately 0.101; the form drag coefficient, 0.160 - all values again at R = 4,000,000. The true skin friction drag coefficient for the Squid is probably lower than the calculated value shown because high velocity flow through the tail was assumed, although observation showed a reduced velocity in this region. The higher

* See reports Section Nos. 6.1-sr-207-933, -938, -1904, -2243

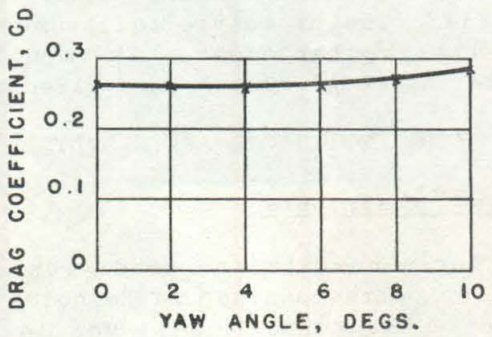

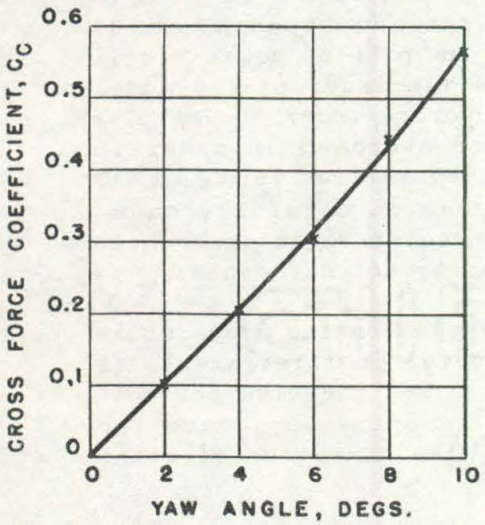

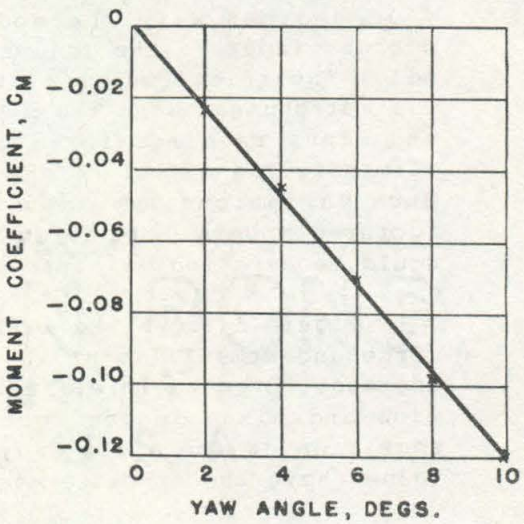

FIG. 3 - 12.75-INCH AS ROCKET
VARIATION OF DRAG, CROSS FORCE, AND MOMENT COEFFICIENTS WITH YAW

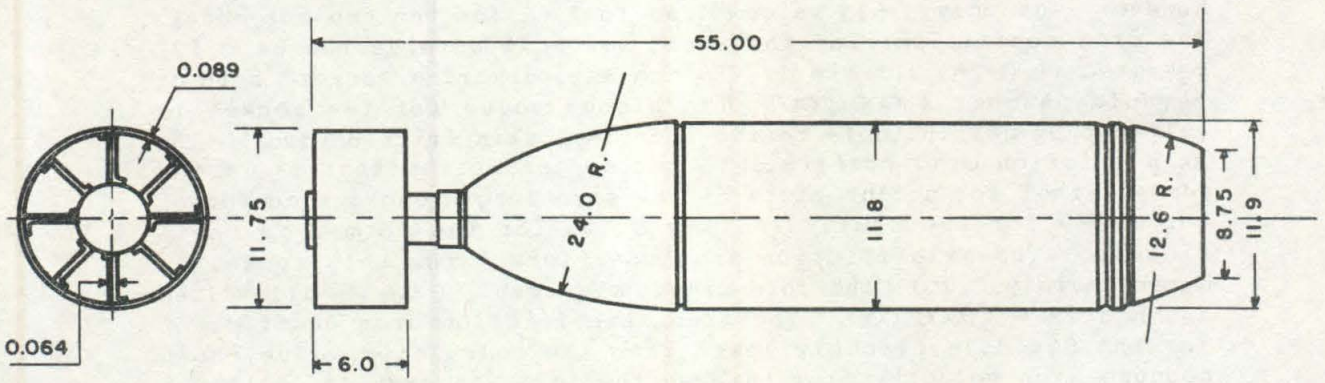

FIG. 4 - PRODUCTION MODEL OF BRITISH SQUID PROJECTILE TYPE C

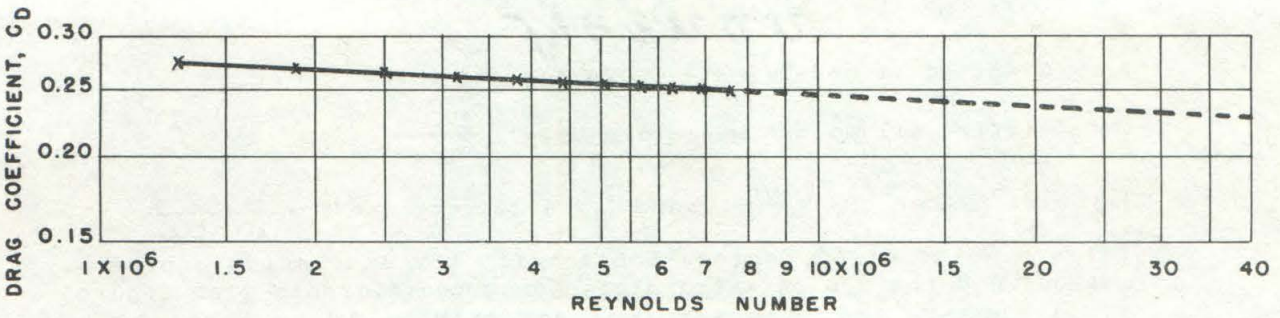

FIG. 5 – 12.75–INCH AS ROCKET
INFLUENCE OF REYNOLDS NUMBER ON DRAG COEFFICIENT

resistance of the rocket seems to be attributable mainly to difference in nose shape and the greater drag of the tail due to more high velocity flow around, and especially through it because of the decreased afterbody interference experienced with the long boom.

The cross force coefficient curve may also be taken as that for the lift coefficient since the projectile is symmetrical about the longitudinal axis. The value at 10 degrees is normal for this type of nose and tail and is practically the same as for the Squid at the same angle.

Both the Squid and this rocket show a considerable degree of static stability, also normal for this design. The rocket moment coefficient has a negative value about 20 per cent greater than the Squid at 10 degrees.

Figure 5 shows the influence of Reynolds number on the drag coefficient. Test velocities were for 10 to 60 ft/sec in increments of 5 ft/sec. The curve shown is the typical straight line for fully turbulent flow conditions. The dash line portion is an extrapolation to higher Reynolds numbers. Any extrapolation in the opposite direction must be made with caution since the transition to laminar flow conditions will disturb the straight line relation. It may be noted that the value of C_D shown in this figure for $R = 4 \times 10^6$ closely checks the values obtained at zero degree yaw, Figure 3.

Terminal Velocity

These data permit calculation of a terminal velocity. The area at the maximum cross section is 127.68 sq. in. and, for the given factor of 2.22 lbs/sq in., the weight in fresh water would be 283.45 lbs. If the projectile weight used for this factor were the loaded weight of 525.2 lbs (which agrees best with our volume calculations), the weight of fresh water displaced is 241.7 lbs. This becomes 248 lbs. for sea water. If the air weight after firing is 504 lbs., the excess weight in sea water is 256 lbs. This value may be substituted for D in the formula

$C_D = \frac{D}{1/2\ \rho\ V^2\ A_D}$ when cavitation has ceased.

A_D = 0.888 sq ft and 1/2 ρ = 0.994 for sea water.

Substituting all values we obtain $V^2 = \frac{290}{C_D}$

Reynolds number, $R_l = \frac{Vl}{\nu}$ where l = 8.13 feet and $\nu = \frac{1.265}{100,000}$ for sea water at 60 degrees Fahrenheit. By successive approximations and the use of extrapolated drag coefficients from Figure 5, it appears that the terminal velocity would be about 35.1 ft/sec. (For 35.1 ft/sec, R = 22,500,000 and for this R, C_D is about 0.235. Then V^2=290/0.235 and V=35.1 ft/sec which checks).

Steady Incipient Cavitation

Cavitation conditions are generally referred to a cavitation parameter, K, a dimensionless number obtained from the formula

$$K = \frac{P_L - P_V}{1/2\ \rho\ V^2}$$

where

P_L = absolute pressure in the indisturbed fluid, lbs/sq ft

P_V = vapor pressure of the fluid, lbs/sq ft

ρ = mass density of fluid, weight in lbs/cu ft divided by acceleration of gravity

V = velocity of projectile in ft/sec

Steady incipient cavitation first appeared on the nose for an average cavitation parameter K value of 1.80. This compares with a value of 2.03 for the Squid. The next appearance of steady incipient cavitation was inside the leading edge of the tail ring for an average of K = 1.26. It showed next on the outside of the ring in small spurs projecting back over the fin joints when K was 0.80. Finally, the complete outside of the ring leading edge showed steady incipient cavitation with a K of 0.64. Afterbody cavitation was not determined since the bubble from the nose obscured the afterbody before cavitation became visible upon it.

Figure 6 is a series of side views, and Figure 7, a corresponding shorter series of top views showing the development of cavitation. Individual views in these figures may be correlated by the K values indicated. It will be noted that the highest K value illustrated is 1.26 although steady incipient cavitation was first noted at K = 1.80. This is because cavitation may be detected by the eye at an earlier stage than one in which it will first show in such photographs. In fact, this picture was taken when steady incipient cavitation was occurring on the inside of

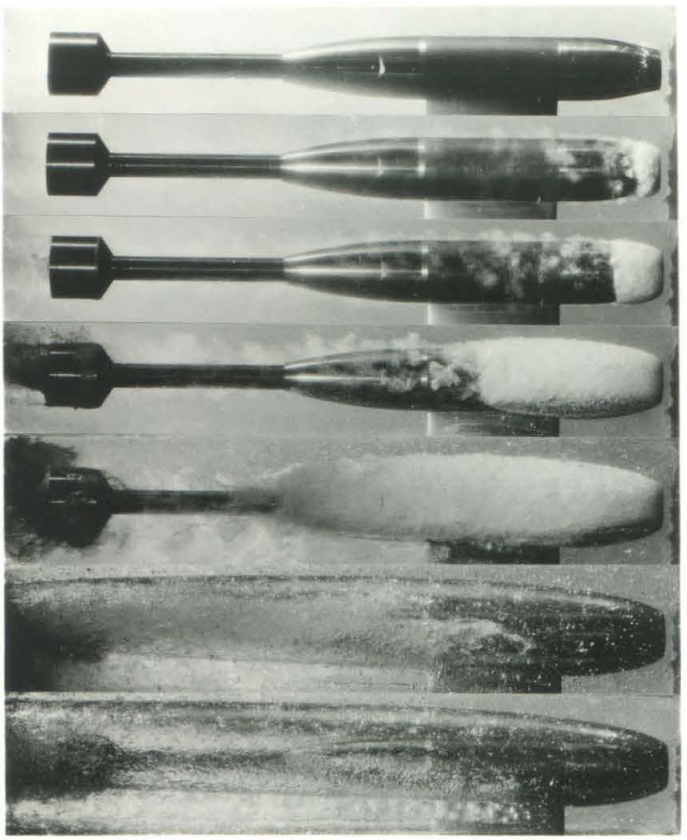

FIG. 6 – SIDE VIEWS

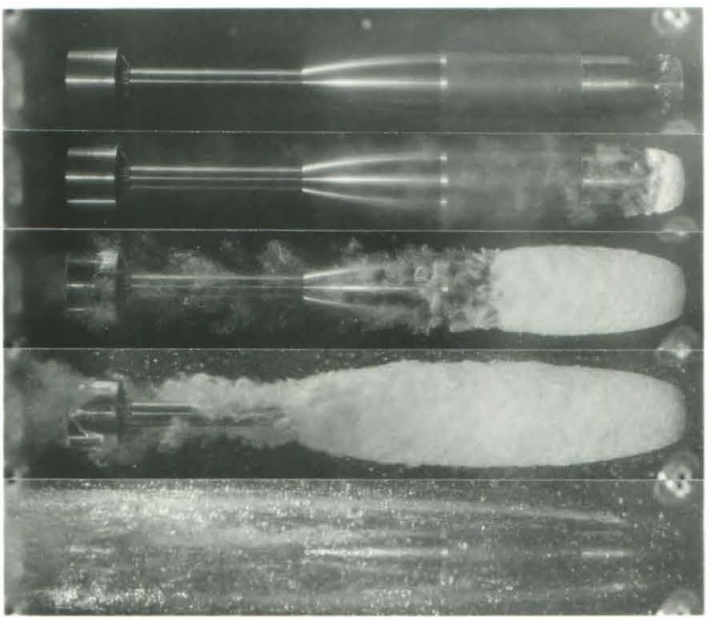

FIG. 7 – TOP VIEWS

DEVELOPMENT OF CAVITATION ON 12.75-INCH AS ROCKET

the ring leading edge. For K = 0.77, nose cavitation is more fully developed and there are clouds of bubbles along the model which have broken away from the collar around the nose. For K = 0.52 (Figure 6), cavitation bubbles may be seen emerging from inside the ring. They show black instead of white because of the nature of the lighting conditions. Pictures for K = 0.31 show cavitation well developed also on the outside of the ring from its leading edge. In Figure 7, K = 0.24, the ring is almost enclosed in a relatively clear bubble. For K = 0.22 and 0.21, the entire model is enclosed in a similarly clear bubble.

The relationship between depth in sea water and cavitation parameter K is given by the formula

$$\text{Depth} = \frac{K V^2}{64.4} - 33.2$$

where depth is in feet and V is in ft/sec.

Force Coefficients with Full Bubble Cavitation

Force coefficients were determined under conditions of full cavitation bubble for yaw angles to $\pm$ 4 degrees, the limit imposed by the magnitude of the drag force. Figure 8 shows the results of

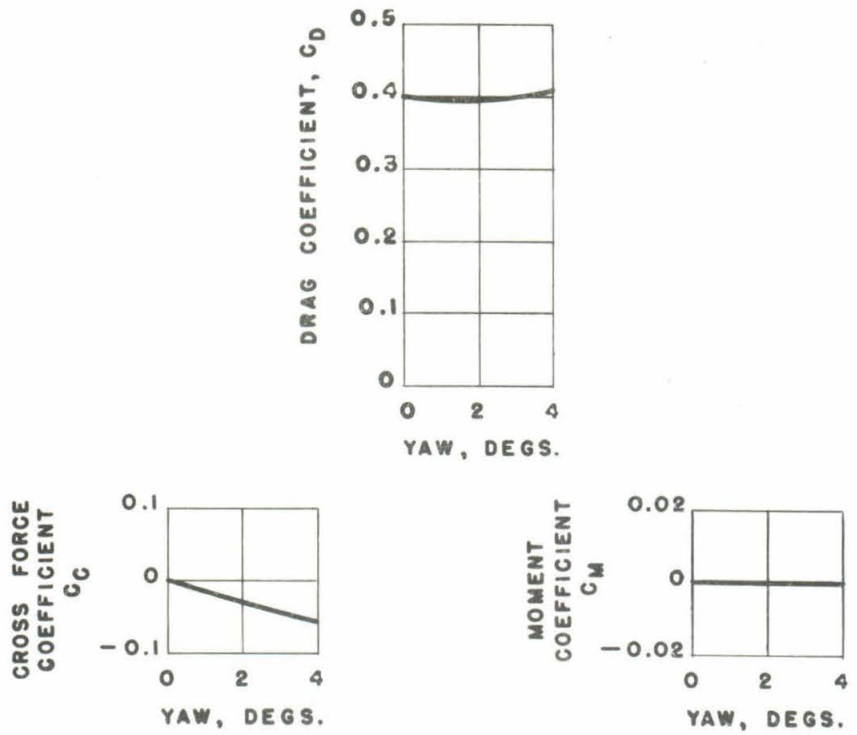

FIG. 8 – 12.75-INCH AS ROCKET
FORCE COEFFICIENTS WITH FULL BUBBLE
V = 50 FT/SEC K = 0.36

of this test. The K value of 0.36, given here for full bubble, differs from the K of 0.21 in Figures 6 and 7 due to the effect of different cavitation shields. The velocity of the water was 50 ft/sec when the data for Figure 8 were obtained. Drag coefficient tests were also made at zero degrees yaw in a full bubble at velocities from 30 to 70 ft/sec, inclusive, at 5 ft/sec increments, which gave an average drag coefficient, C_D, of 0.39 as compared to the value of 0.40 for 50 ft/sec shown in Figure 8. The average K value of these runs was 0.36. All values were corrected for shield interference. The drag coefficient was not, of course in this case, corrected for horizontal buoyancy.

The drag coefficient in the full bubble stage may be considered to be due entirely to form drag. It checks with previous tests of a truncated ogive (edges rounded) in a full bubble and comparable K.*

The cross force coefficient shows a small negative value as may be expected under these conditions for a nose of this type. The most nearly similar nose previously tested, a square-end cylinder, gave a C_C of -0.06 at 3 degrees compared to -0.045 at the same angle for this nose.

The moment coefficient, C_M, (about the C.G.) has a zero value, within observational errors, to $\pm$ 4 degrees. A drag force D, on a flat faced nose with a yaw angle α, has a small lateral component, D tan α, which exerts a destabilizing effect when the center of pressure is forward of the center of gravity. The negative cross force acts in the opposite direction and is sufficient to offset the destabilizing effect of the drag and provide a small stabilizing effect, but, in this case, too small to appear in the moment measurements.

Polarized Light Flume Diagram

Figure 9 is a flow diagram obtained from observation of conditions in the Polarized Light Flume, with the projectile at 0 degrees and 10 degrees pitch. Since the projectile is symmetrical about its longitudinal axis, conditions for 10-degree yaw would be as shown for 10-degree pitch. The flow conditions revealed (at a velocity of about 5 feet per second) are in accord with expectations for this shape. The blunt nose produces some disturbance in the flow, immediately aft, which is symmetrical for zero angle of presentation and greater on the top side, for upward nose pitch. This disturbance seems to be somewhat larger than for the Squid nose previously mentioned in comparison. It is offset to some degree by smaller afterbody disturbances resulting from a more streamlined form. The zone of disturbance at the boom end is normal for such conditions.

* "Hydrodynamic Forces Resulting from Cavitation on Underwater Bodies" HML Report ND-31.2, Section No. 6.1-sr207-2242, July 21, 1945.

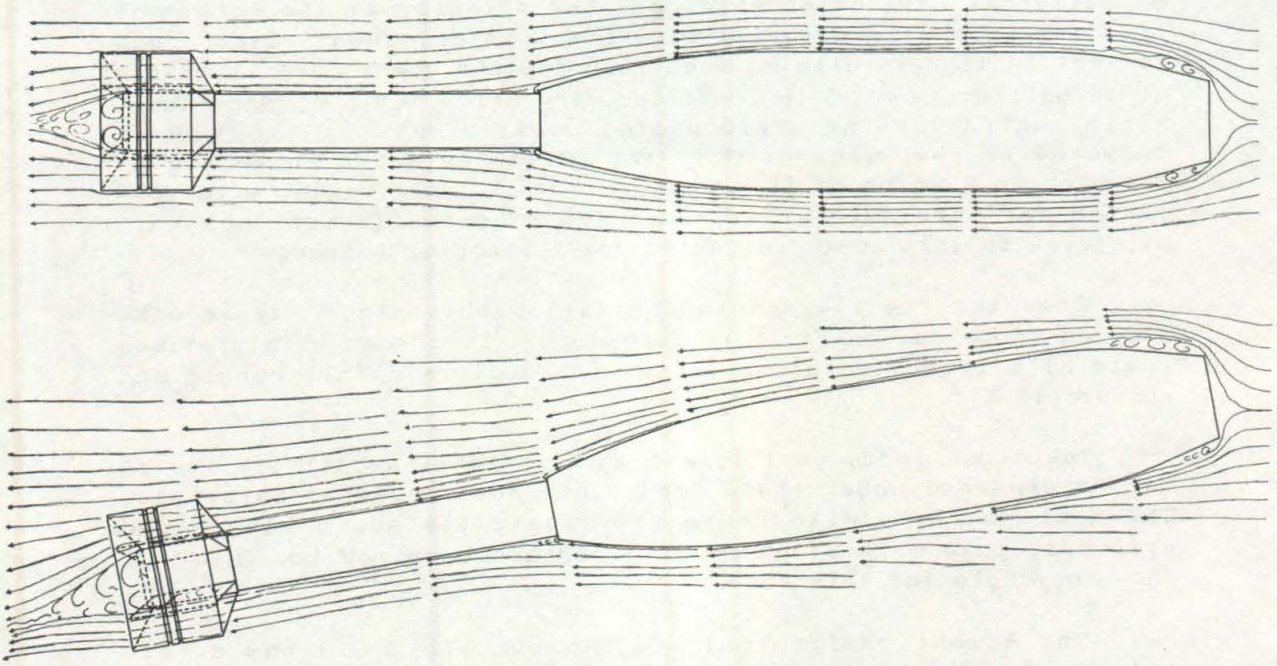

FIG. 9 – POLARIZED LIGHT FLUME DIAGRAMS
0^{o} AND 10^{o} PITCH

PART II

PURPOSE

The purpose of the additional investigation was to obtain an increase in the sinking rate by nose modification only, which would retain a flat face not less than 6.4 inches in diameter (prototype dimension) and to make tests similar to those in Part I with the modified forms.

ESTIMATED CONTRIBUTION OF COMPONENTS TO DRAG

An analysis of the shape and dimensions of the original projectile design caused us to estimate the percentage contribution of the various components to the total drag as follows:

Projectile Component	Drag Skin Friction %	Form %	Total %
Cylindrical body section	9	1	10
Boom	6	1	7
Afterbody	9	4	13
Tail	10	10	20
Nose	5	45	50
Total	39	61	100

This indicated that a considerable improvement was possible by reduction of the (original) nose form drag. The adverse factors in the original nose were surmised to be (1) the sharp edge formed by junction of the flat face and cone section, and (2) the cone section itself. A new nose was designed, in which these were eliminated, by extending the orignial ogive until it formed the minimum diameter (1/2 D) flat face and by rounding the corner with a radius equivalent to 0.45 inch in the full-scale projectile. (It is referred to herein as Nose No. 162). This infringed slightly on the 1/2 D restriction, but a study of original drawings indicated that it might be permissible. Subsequent tests showed that a similar nose without any infringement would give results substantially as good, since the diameter of the flat face is not critical for drag until it becomes much larger (above 3/4D).

ADDITIONAL NOSES SELECTED FOR TEST

During the period in which the new nose was being designed and constructed, tests were begun with stock model noses which

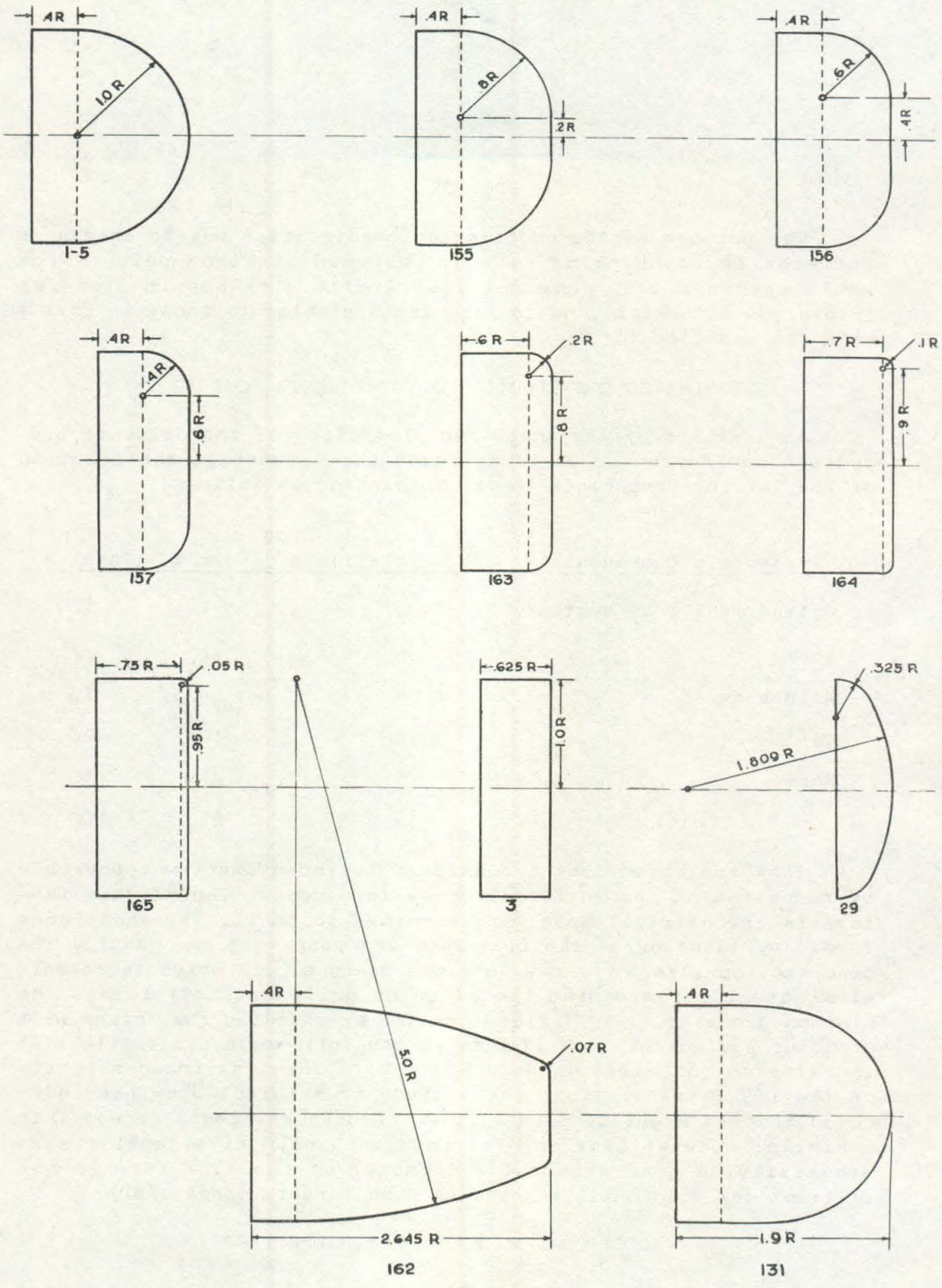

FIG. 10

were considered promising. The first results were so encouraging that a considerable series of noses was scheduled in order to evaluate trends. The final program contained eleven noses in addition to the original previously tested.

Eight of the noses formed a series with flat faces changing in diameter from 0 to 1 caliber and with the profile, between the edge of the flat face and cylindrical body, a quadrant circular arc of suitable radius. The nose with 0-caliber diameter flat face was thus a hemisphere and, for a 1-caliber diameter flat face, it became a "square" nose. This series is shown in the top three rows of Figure 10, the progression being from hemisphere to square. It should be noted that each of these outlines includes part of a cylindrical body section which is not part of the nose, considered hydrodynamically. They were designed in this manner to avoid difficulties which arise in cavitation measurements when there is a separation joint at the junction of a curved and straight section and, in some cases, to give sufficient length for assembly purposes. Nose No. 29 is a two-arc nose used primarily for check purposes, and in the bottom row (at left), the modified original described above. The last nose, No. 131, shows the model drawing of one with special profile also tested for checking. The profile of Nose 131 is calculated from the equation $(X/1.5)^3 + (Y)^2 = 1$. The numbers shown with each nose are for identification purposes.

TEST UNIFORMITY CONTROL

The over-all length and support point were the same with each nose as for the original model. This was obtained by alteration of the length of cylindrical body sections. All tests were made under the same conditions and similar corrections were applied to the test data. Yaw tests, described below, were made with a velocity of 32 feet per second.

RESULTS FOR SPEED-DRAG TESTS

Figure 11 shows the measured (solid line) and extrapolated (dash line) values of the drag coefficient with changing Reynolds number for the noses tested, except 163, 164, and 165. The results have been divided into two parts to reduce the confusion of multiplicity. The upper group has been labelled "Primary Noses" because they are of greater and more direct interest than the "Secondary Noses" grouped below. The line at the extreme top is the completely square nose with a flat face diameter of one caliber, unrounded edge (No. 3). Its important characteristics are the high values of the drag coefficient and the relatively small decline as Reynolds number increases. This decline is only 8 per cent from $R = 3 \times 10^6$ to 3×10^7 for the extrapolation indicated. It has been included in the primary group for comparison with the line for the original nose (No. 161) where, again, the small reduction in the drag coefficient is obvious. In this case, it is 10.7 per cent between the same limits and results from the "squareness", that is, the sharp edge and cone section, primarily,

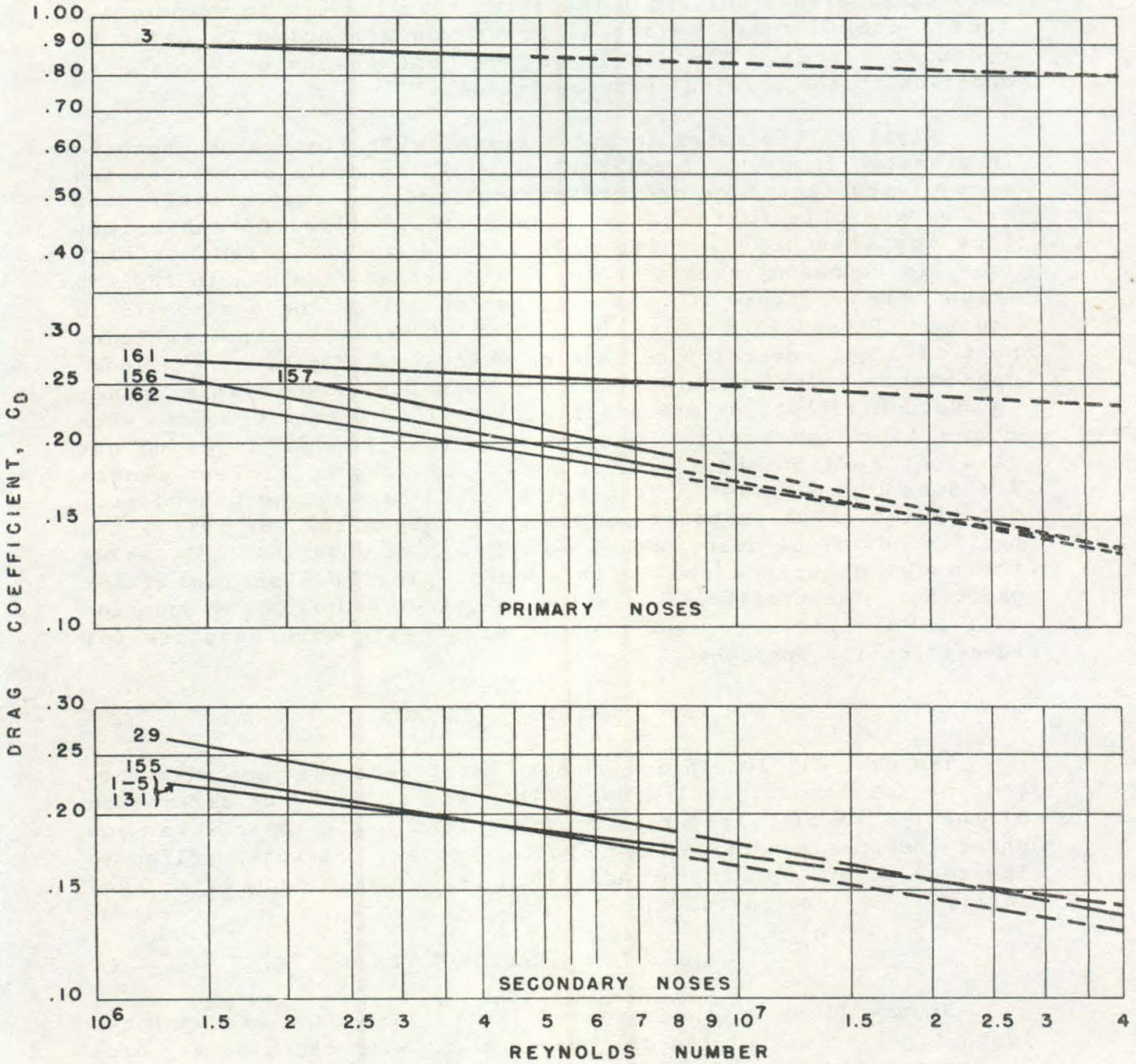

FIG. 11 – INFLUENCE OF REYNOLDS NUMBER ON DRAG COEFFICIENT OF NOSES TESTED WITH 12.75-INCH AS ROCKET

and the flat face very secondarily. This is apparent from a consideration of the other noses in this group. Nose 157 has a flat face of 0.6-caliber diameter, almost the same as for Nose 161, but its quadrant circle curvature permits a 39.5 per cent decline in C_D over the same range of R. Nose 162, the modified original, gives 32.3 per cent, but it is favorably comparable to No. 157 because of lower values at all R numbers in this range. Nose 156 has a flat face of 0.4-caliber diameter and quadrant circle fill being, thus, the same amount smaller than the 0.5-caliber diameter specified in the basic letter. The decline for No. 156 is

37.2 per cent and the value at full scale R, the lowest (0.138 at 3 x 10^7). A nose of this design with a flat face diameter of 0.5 caliber would, presumably, have a line lying half way between those for No. 156 and No. 157 and give a C_D of 0.140 as compared to 0.138 and 0.142, respectively, and corresponding to a difference of 1/3 foot per second in terminal velocity.

ESTIMATED TERMINAL VELOCITIES

These curves permit calculation of estimated terminal velocities. They are given, below, for the assumptions, (1) that there is no water in the discharged motor tube, and (2) that it contains 23.7 pounds of sea water. Average water temperature assumed: 60° F.

Nose Numbers	Terminal Velocity, ft/sec No Water	Water	R
3 (square)	18.6	19.5	12.5 x 10^6
161 (original)	35.2	36.8	23.6
162 (modified)	45.4	47.7	30.5
157 (0.6 flat face)	44.9	47.4	30.4
156 (0.4 flat face)	45.7	48.0	30.8
155 (0.2 flat face)	46.3	48.5	31.1
29	44.7	47.0	30.2
131 and 1-5 (HS)	44.1	46.4	29.7

If the values obtained for the original design are taken as 100 per cent, the others are as follows:

Nose	Per cent
3 (square)	53
161 (original)	100
162 (modified)	129.5
157 (0.6 flat face)	128.8
156 (0.4 flat face)	130.4
155 (0.2 flat face)	131.7
29	127.6
131 and 1-5 (HS)	126.0

(Increase requested was 108.5)

It is apparent that, after excluding the noses which do not conform to the restrictions imposed, Noses No. 157 and No. 162 give estimated terminal velocities so well above the 40 feet per second desired as to leave adequate margin for errors of measurement and extrapolation, scale effect, and lower sea water temperatures. Yaw tests were made for all noses except Nos. 163, 164, and 165 (and reported below), but Nos. 157 and 162 only were selected for cavitation and force cavitation measurements. While these two noses appear to be equally suitable from the viewpoint of terminal velocity, their different shapes afford additional opportunity for selection on grounds of maximum range, ricochet characteristics, cavitation, and performance in entry bubble.

It may be noted, at this point, that these noses eliminate approximately 42 of the 45 per cent estimated as due to form drag of the original nose (at full-scale Reynolds number). These tests indicate, in any case, that relatively small improvement could be made in the drag coefficient with any other nose used in conjunction with other parts which remained unchanged. However, it is not proper to assume that these noses would remain equally suitable, or the best, if other parts were changed, since the total effect is due to an intimate relation of all parts.

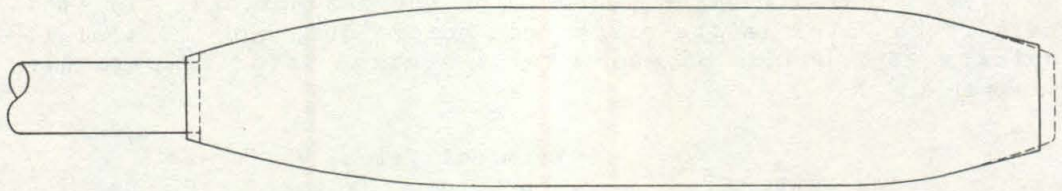

FIG. 12 – OUTLINE OF 12.75–INCH TYPE X10 ANTISUBMARINE ROCKET WITH MODIFICATIONS

Mention is made here of the fact that a small ring was added to the afterbody (see Figure 12) extending its contour to the boom and used in the test of Nose No. 162. Its contribution to the results appeared to be negligible.

GENERALIZED NOSE DESIGN DATA

The test of Nose 163, which had a flat face diameter of 0.8 caliber, produced results which have important aspects. Reference to Figure 13 shows that the drag coefficient was nearly twice that of Nose 157 (with a 0.6-caliber flat face) at $R = 1.5 \times 10^6$; that it declined at a slower rate with increasing Reynolds number until it passed $R = 4 \times 10^6$, whereupon it took a sharp dive and closely approximated, thereafter, the values for No. 157 (above $R = 5 \times 10^6$); and that, when velocities were decreased, the line for Nose 163 followed that of No. 157 to $R = 2.7 \times 10^6$ before it returned, sharply, to the high value branch. This action forms a hysteresis loop. The sudden transition indicates, of course, a radical change in flow separation and is analogous to that observed for a sphere at R about 0.3×10^6. The test of No. 157 indicated that a similar effect could be noted only at Reynolds numbers below 1.5×10^6.

Noses No. 164 (0.90) and No. 165 (0.95) gave progressively higher values of C_D, and declines with increase in R, which approximated that for a completely square nose (No. 3). No sharp decline, similar to that for No. 163, was obtained up to $R = 8 \times 10^6$, the present tunnel measurement limit. It may be that a transition similar to that for No. 163 will occur with these other noses at sufficiently higher Reynolds numbers. However, it seems unlikely that the original nose (No. 161) on the full-scale projectile would give a smaller C_D from such a cause than that previously indicated by the straight line extrapolation from our tests, since the point of separation occurs and remains at the sharp edge.

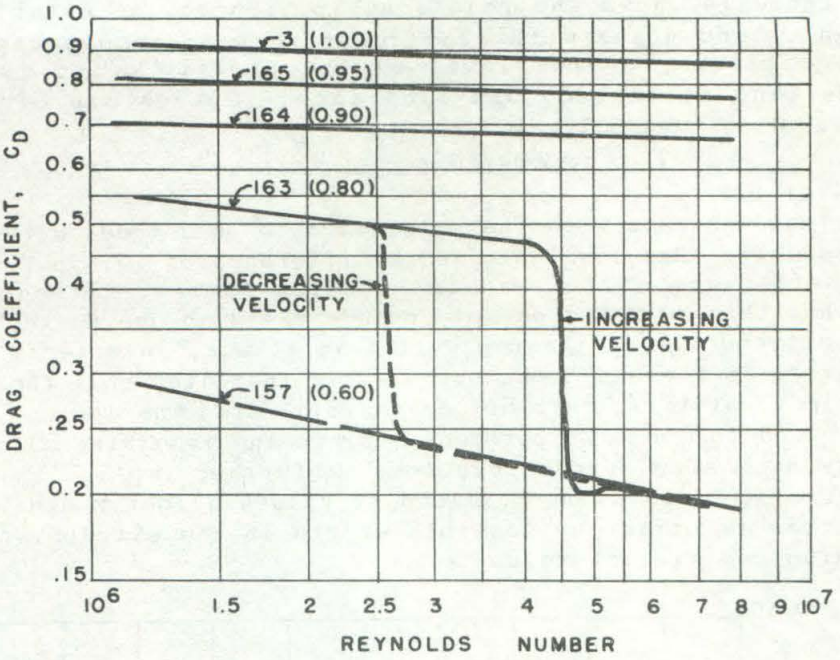

FIG. 13 — INFLUENCE OF REYNOLDS NUMBER ON DRAG COEFFICIENT OF 12.75-INCH AS ROCKET WITH NOSES NOS. 157, 163, 164, 165, AND 3

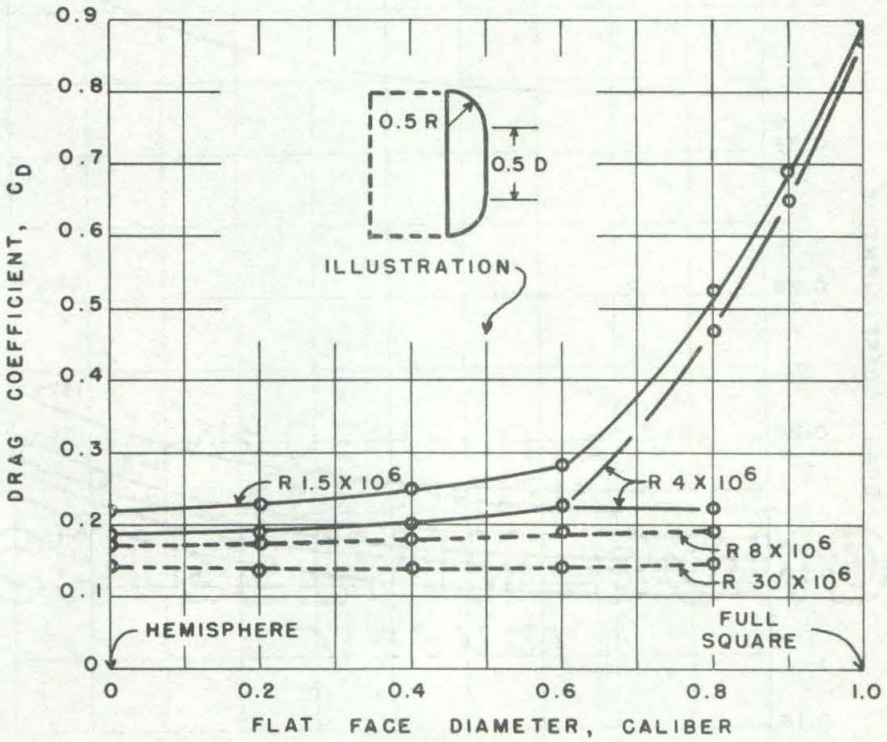

FIG. 14 — INFLUENCE OF EDGE ROUNDING OF NOSE ON DRAG COEFFICIENT OF 12.75-INCH AS ROCKET

These noses had a flat face, with diameters indicated by values on the abscissa scale, joined to the body by quarter-circle segments tangent to flat face and body.

Figure 14 shows the relationship, insofar as established, between C_D and noses with flat faces varying in diameter from 0 to 1 caliber, the remainder of the profile being quadrant circles tangent to body and flat face. Curves are given for R = (1.5, 4, 8, and 30) x 10^6.

CONTRIBUTION OF TAIL

A test was made with the original nose on a model without the tail assembly. Results indicated a difference of 19.5 per cent in drag coefficient at full-scale Reynolds number. It should be noted that this amount does not include the drag due to turbulence at the extreme aft of the projectile as it was, in effect, merely transferred to the end of the boom. This indicates that the original estimate of tail contribution to total drag was low and should be increased to about 25 per cent. Since the remaining allowances for form drag seem irreducibly low, it further implies that skin friction drag assumptions may lead to values slightly high. This implication is offset by possible errors in the extrapolation of total drag coefficient values.

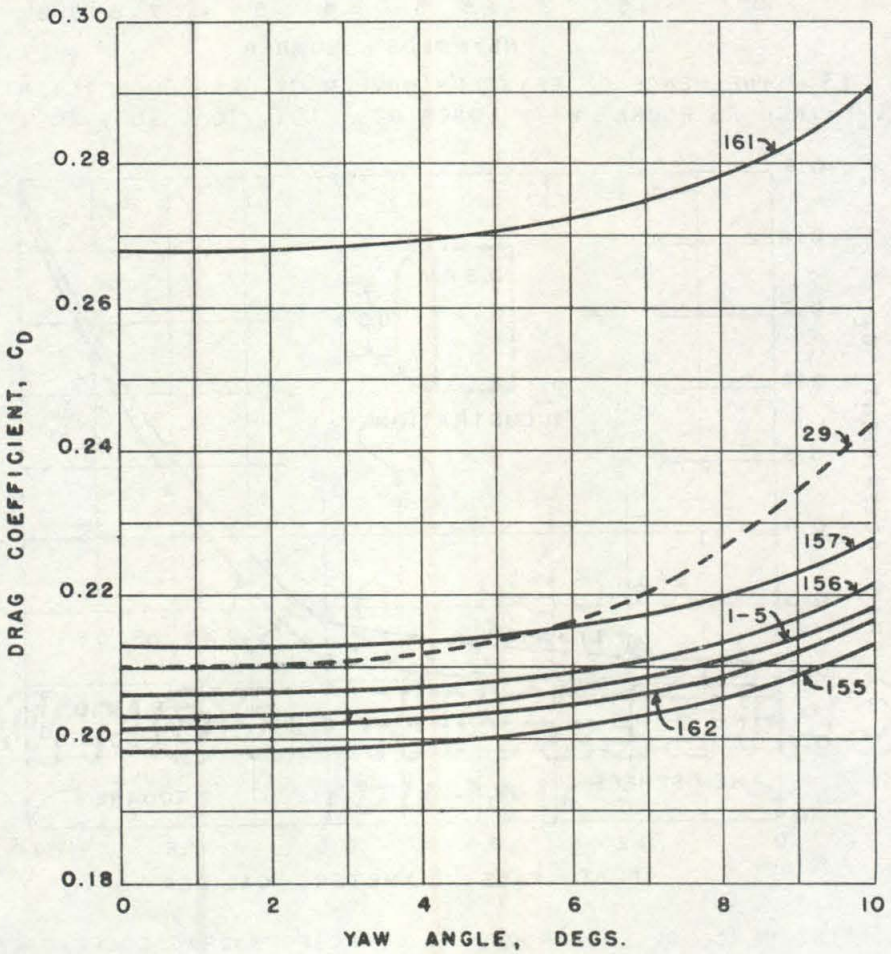

FIG. 15 – INFLUENCE OF YAW ANGLE ON DRAG COEFFICIENT OF 12.75-INCH AS ROCKET WITH VARIOUS NOSES

Results of Yaw Tests

Figure 15 shows the influence of yaw angle on the drag coefficient of the 12.75-inch AS Rocket model with the various noses. The unusual scale for the drag coefficient has been used to give a reasonable separation of the curves. "Family" noses appear to have the same general trend, while those which do not belong, as No. 29, are different. No curve is shown for No. 131 as the data are inconsistent and the test was not repeated due to the relative unimportance of this nose. No curve is shown for No. 3 (square) as it was used for a check point. (Value at 0° = 0.88; 10° = 0.98).

Figure 16 shows the influence of yaw angle on the cross force coefficient with the original nose (161). No others are shown because differences are too small. The maximum differences were at 10° yaw and the absolute values were as follows:

Nose No.	C_C at 10°
157	.586
161, 155, 1-5	.575
162	.565
29	.560
156	.550
131, 3 (erratic)	.540

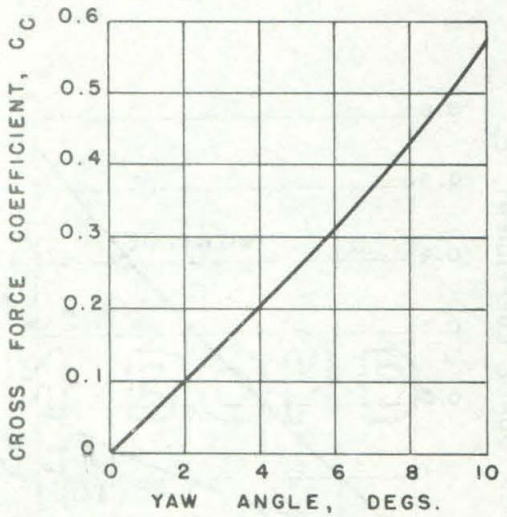

FIG. 16 – INFLUENCE OF YAW ANGLE ON CROSS FORCE COEFFICIENT OF 12.75-INCH AS ROCKET

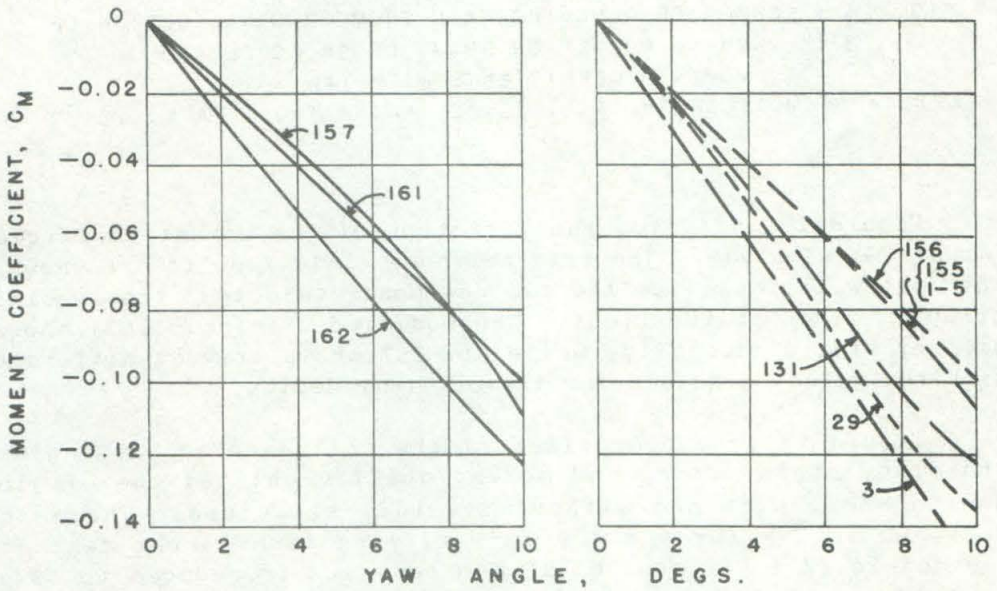

FIG. 17 – INFLUENCE OF YAW ANGLE ON MOMENT COEFFICIENT OF 12.75-INCH AS ROCKET WITH VARIOUS NOSES

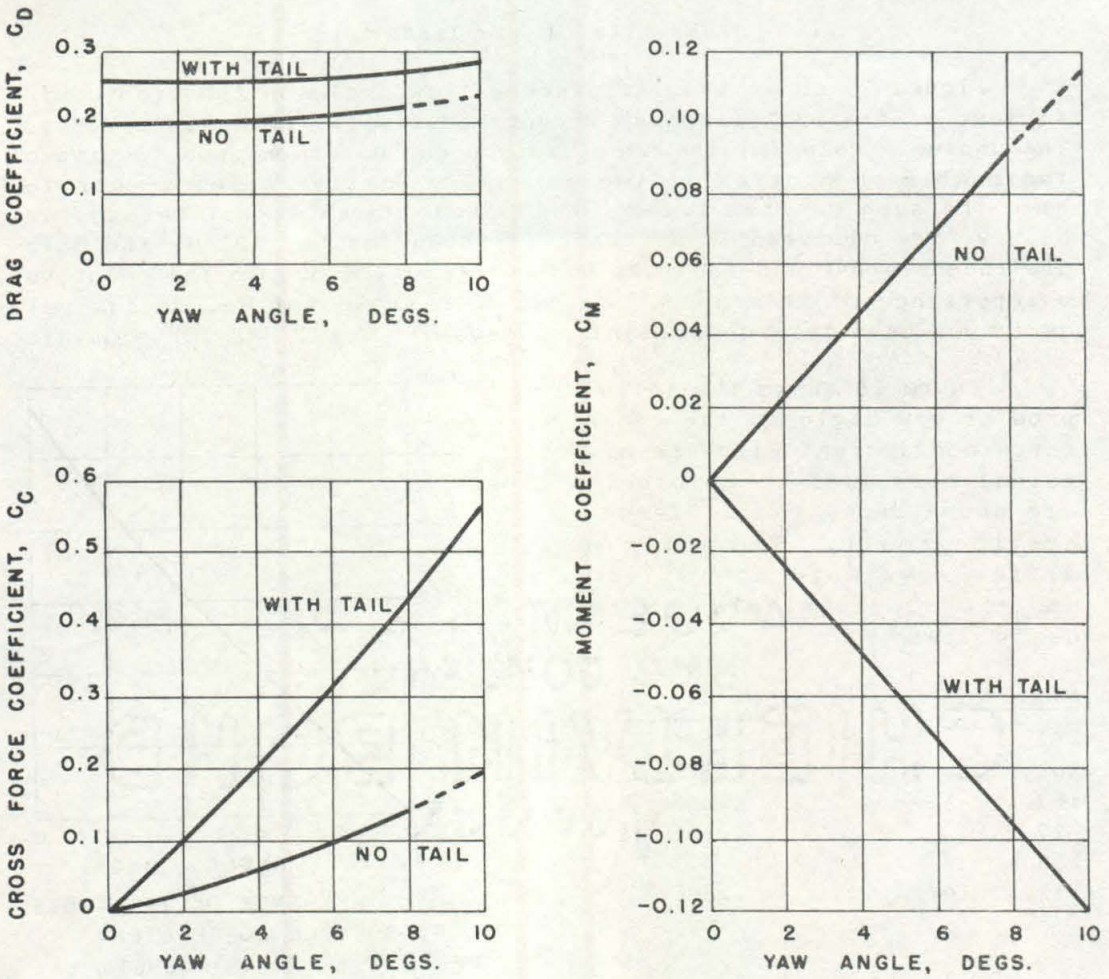

FIG. 18 – EFFECT OF REMOVING TAIL FROM ORIGINAL DESIGN OF 12.75–INCH AS ROCKET ON DRAG, CROSS FORCE AND MOMENT COEFFICIENTS WITH YAW
LENGTH OF MODEL WITH TAIL, 15.31 IN.; WITHOUT TAIL, 13.25 IN.

Figure 17 indicates the variation of the moment coefficient (about CG) with yaw. The original nose (161) results are shown at the left with those for the two new noses selected; the remaining group is given at the right. The modified original (162) shows a greater static stability, while No. 157 shows trivial differences with the values obtained for the original design.

Figure 18 is a comparison of the influence of yaw angle on the drag, cross force, and moment coefficients of the original design model with and without its tail structure. There is a decrease in C_D (for $R = 4 \times 10^6$) varying from 24 per cent at 0 degrees to 17.5 per cent at 10 degrees. C_C is reduced to 35 per cent of its normal value at 10 degrees, while the effect on C_M is such as to indicate marked static instability.

INCIPIENT CAVITATION

Test of the model with Noses 157 and 162 were made to determine incipient cavitation values. They are listed below and compared with results for the original nose (161).

Location	K Values for Model with Nose		
	157	162	161
	Incipient Cavitation		
Nose	1.65	(0.55) (0.37)	1.80
Inside leading edge of ring	1.11	1.11	1.26
Outside ring at fin junction	1.02	1.00	0.80
Complete outside of leading edge of ring	0.66	0.76	0.64
Afterbody	Obscured	0.325	Obscured

Nose bubble, length on model, calibers	Length	K Value	
	0.75	0.68	
	2.0	0.39	0.211
	4.0	0.31	0.187
	6.0	0.28	0.172
	8.0	0.265	0.171
	15.0	0.258	0.167

It may be seen that steady incipient cavitation appears first on the nose for Nos. 161 and 157 (K = 1.80 and 1.65, respectively), but on the inside leading edge of the ring when Nose 162 is used (at K = 1.11). Steady incipient cavitation is not established on No. 162 until K is reduced to 0.55 when it shows immediately aft of the nose edge rounding. When K is reduced to 0.37, the nose ogive also starts to cavitate at approximately the midpoint. It also became possible to determine the incipient K value for the afterbody (0.325), previously obscured by cavitation from the other noses.

It may be concluded that, as regards cavitation, Nose 157 is slightly better than the original (161), while the modified original (162) is so much better as to be well below other components of the projectile.

Figures 19 and 20 present side and top views of the development of cavitation with Nose 157. The first photograph in each figure shows conditions for K = 1.55. Cavitation has progressed much farther in the second picture, where K = 0.56. Bubble patches aft of the nose collar are fragments broken away from it. The outside of the leading edge of the ring is cavitating but the stream from the ring comes mainly from cavitation on the inside of the leading edge. Subsequent pictures show development to a full length bubble in the picture next to the bottom, the latter being considerably longer.

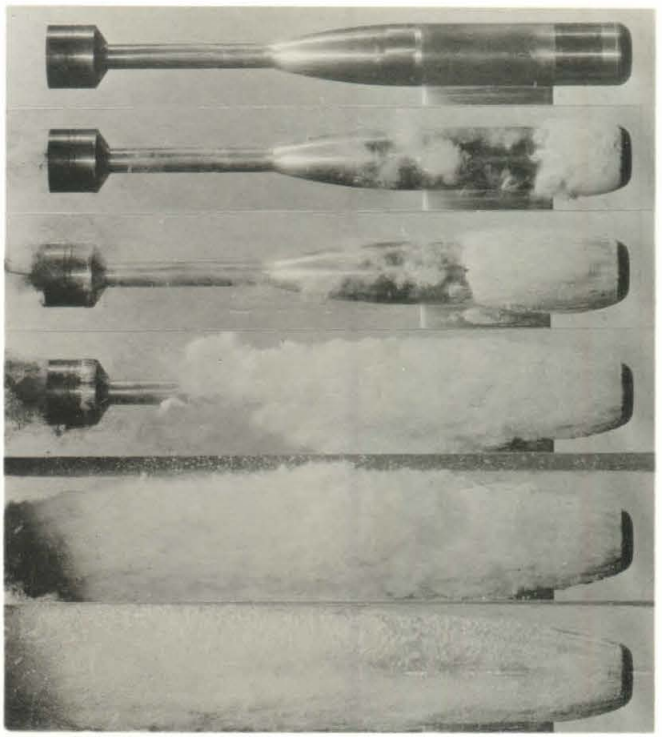

FIG. 19 – SIDE VIEWS

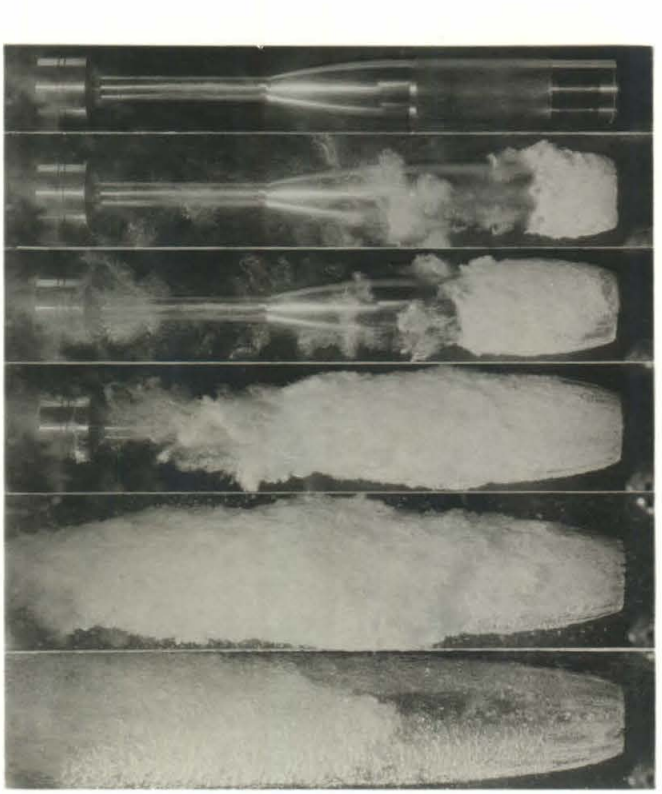

FIG. 20 – TOP VIEWS

DEVELOPMENT OF CAVITATION ON 12.75 – INCH AS ROCKET WITH NOSE NO. 157

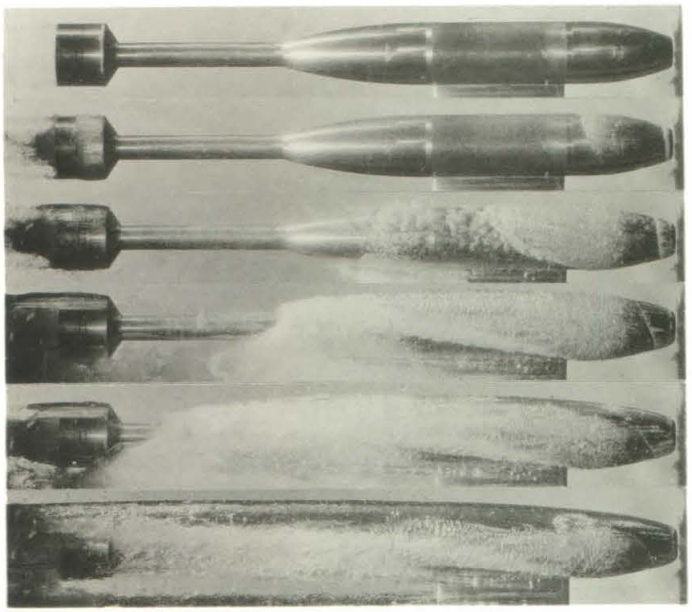

FIG. 21 – SIDE VIEWS

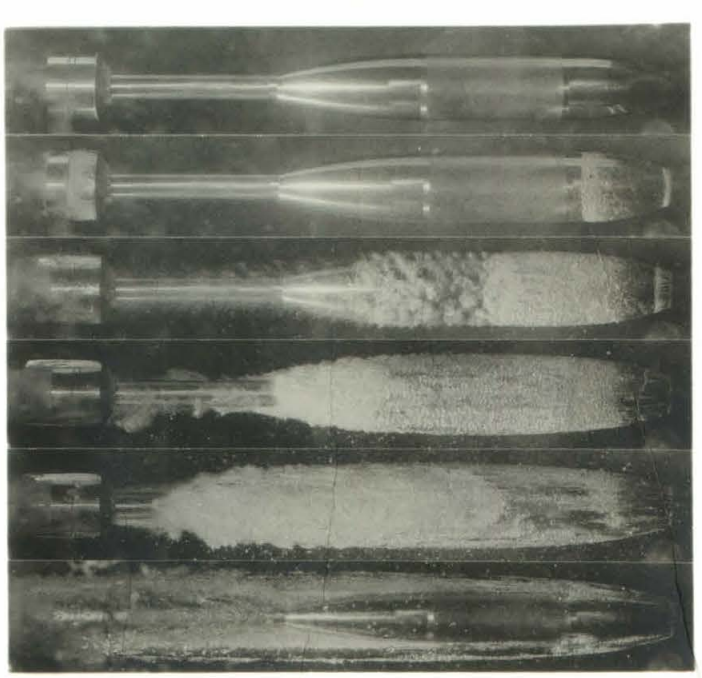

FIG. 22 – TOP VIEWS

DEVELOPMENT OF CAVITATION ON 12.75-INCH AS ROCKET WITH NOSE NO. 162

Figures 21 and 22 are similar side and top views of cavitation development with Nose 162. Steady incipient cavitation on the nose was visible to the eye when the first picture (K = 0.55) in each of these series was taken, but hardly shows in the photographs. The cavitation on the leading edge of the ring is plainly visible. The second set shows the two zones of cavitation produced by this nose (K = 0.31). The difference in type of cavitation bubbles produced by these noses may be seen by comparing Figures 19 and 20 with 21 and 22. Nose 157 gives the "fine-grained" type, very small bubbles, densely packed, while Nose 162 produces larger bubbles, widely spaced, and characteristic of more highly streamlined shapes. The top of the nearly full bubble has cleared sufficiently to give a good view of the projectile body in the bottom print of Figure 22.

FORCE COEFFICIENTS, CAVITATION

Figure 23 gives the results for the influence of yaw angle on the force coefficients when the model is in a cavitation bubble.

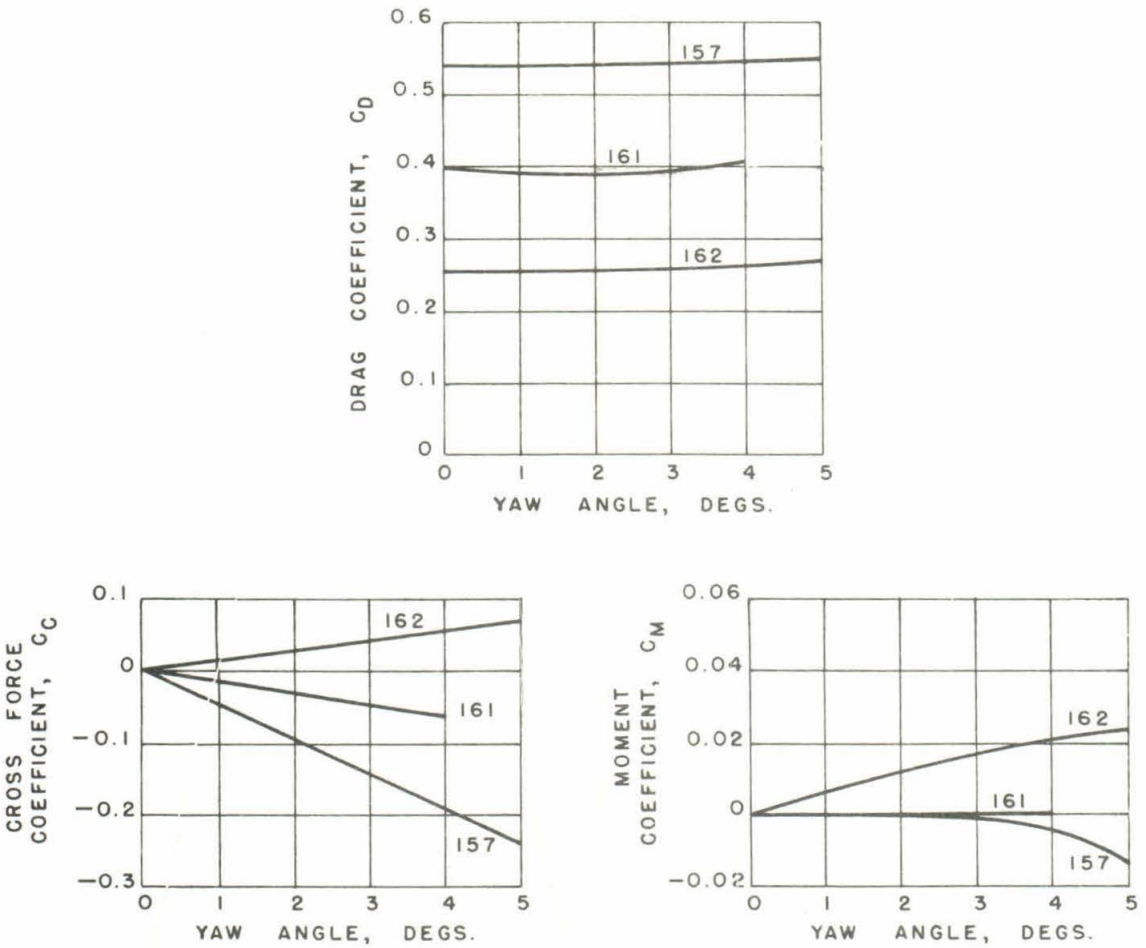

FIG. 23 — INFLUENCE OF YAW ANGLE ON DRAG, CROSS FORCE AND MOMENT COEFFICIENTS FOR MODELS OF 12.75-INCH AS ROCKET WITH NOSES NOS. 157, 161, AND 162 WHEN IN A CAVITATION BUBBLE

The sharp edged nose of the original design made full bubble cavitation possible, but the removal of the sharp edge made it impossible to obtain in the present tunnel. There remains, then, some question as to the strict comparability of the results shown here for Noses 157 and 162 with those for Nose 161. However, the cavitation bubble obtained was such as to lead to the belief that the general relationship is correct.

The relatively high negative cross force for Nose 157 tends to counteract the destabilizing effect of the drag and is reflected in a small degree of static stability shown by the moment curve.